Identification of Glucose Transport Modulators In Vitro and Method for Their Deep Learning Neural Network Behavioral Evaluation in Glucose Transporter 1–Deficient Mice[S]

Gauri Kathote,[1] Qian Ma,[1] Gustavo Angulo, Hong Chen, Vikram Jakkamsetti, Aksharkumar Dobariya, Levi B. Good, Bruce Posner, Jason Y. Park, and ⓘ Juan M. Pascual

Rare Brain Disorders Program, Department of Neurology (G.K., Q.M., G.A., V.J., A.D., L.B.G., J.M.P.), Department of Biochemistry (H.C., B.P.), Department of Pathology (J.Y.P.), Department of Physiology (J.M.P.), Department of Pediatrics (J.M.P.), and Eugene McDermott Center for Human Growth & Development/Center for Human Genetics (J.Y.P., J.M.P.), University of Texas Southwestern Medical Center, Dallas, Texas.

ABSTRACT

Metabolic flux augmentation via glucose transport activation may be desirable in glucose transporter 1 (Glut1) deficiency syndrome (G1D) and dementia, whereas suppression might prove useful in cancer. Using lung adenocarcinoma cells that predominantly express Glut1 relative to other glucose transporters, we screened 9,646 compounds for effects on the accumulation of an extracellularly applied fluorescent glucose analog. Five drugs currently prescribed for unrelated indications or preclinically characterized robustly enhanced intracellular fluorescence. Additionally identified were 37 novel activating and nine inhibitory compounds lacking previous biologic characterization. Because few glucose-related mechanistic or pharmacological studies were available for these compounds, we developed a method to quantify G1D mouse behavior to infer potential therapeutic value. To this end, we designed a five-track apparatus to record and evaluate spontaneous locomotion videos. We applied this to a G1D mouse model that replicates the ataxia and other manifestations cardinal to the human disorder. Because the first two drugs that we examined in this manner (baclofen and acetazolamide) exerted various impacts on several gait aspects, we used deep learning neural networks to more comprehensively assess drug effects. Using this method, 49 locomotor parameters differentiated G1D from control mice. Thus, we used parameter modifiability to quantify efficacy on gait. We tested this by measuring the effects of saline as control and glucose as G1D therapy. The results indicate that this in vivo approach can estimate preclinical suitability from the perspective of G1D locomotion. This justifies the use of this method to evaluate our drugs or other interventions and sort candidates for further investigation.

SIGNIFICANCE STATEMENT

There are few or no activators and few clinical inhibitors of glucose transport. Using Glut1-rich cells exposed to a glucose analog, we identified, in highthroughput fashion, a series of novel modulators. Some were drugs used to modify unrelated processes and some represented large but little studied chemical compound families. To facilitate their preclinical efficacy characterization regardless of potential mechanism of action, we developed a gait testing platform for deep learning neural network analysis of drug impact on Glut1-deficient mouse locomotion.

Introduction

Glucose is the principal metabolic fuel used by cells throughout the organism. This is particularly relevant in neural and cancer cells, which exhibit elevated glycolysis rates associated with normal functional activity or with survival and proliferation, respectively. Glucose enters many of these cells predominantly via the facilitative membrane transporter Glut1 (glucose transporter 1). This transporter is subject to haploinsufficiency, downregulation, or upregulation in neurologic and oncological diseases. For example, diminished Glut1 expression and brain glucose content is a hallmark of glucose transporter 1 deficiency syndrome (G1D) (Pascual et al., 2002; Rajasekaran et al., 2022) and various types of dementia (Rosenberg and Pascual, 2020), whereas elevated Glut1 expression can signify cancer growth, invasiveness, or adaptation (DeBerardinis and Chandel, 2016). Thus, there is a longstanding interest in stimulating or suppressing glucose flux into neural or cancer cells via Glut1 or other mechanisms.

ABBREVIATIONS: FPS, frames per second; G1D, glucose transporter 1 deficiency syndrome; Glut1, glucose transporter 1; HTS, high-throughput screening; LDA, linear discriminant analysis; MANOVA, multivariate analysis of variance; 2-NBDG, 2[N-(7-nitrobenz-2-oxa-1, 2-diaxol-4-yl)amino]-2-deoxyglucose; NIH, National Institutes of Health; PCA, principal component analysis; RZ, robust Z; UT, University of Texas; WT, wild-type.

G1D is often associated with glucose-responsive encephalopathy (Pascual and Ronen, 2015). The disease usually stems from partial or complete loss of function (or haploinsufficiency) of only one copy of the *slc2a1* gene (Pascual et al., 2008). Despite the presence of other glucose transporters in the brain, Glut1 virtually constitutes the obligate or principal facilitator of glucose flux across red blood, blood-brain barrier, and cerebral glial cells. Consequently, in G1D there is most likely progressively decreased glucose flux through a series of cellular compartments that span from circulating red blood cells or plasma to neural cells. This results in metabolic substrate deprivation of the brain (Marin-Valencia et al., 2013).

The clinical expression of G1D represents a multiform neurologic disease with infantile onset. Despite constituting a disorder studied by numerous investigators (Klepper et al., 2020) and one for which an informative stable DNA antisense mouse model exists (Marin-Valencia et al., 2012, 2013; Rajasekaran et al., 2022), G1D has proven incompletely or inadequately treatable. Paradoxically, most antiseizure drugs aggravate or are ineffective against seizures when they are present (Wang et al., 1993; Rajasekaran et al., 2022). Current therapies thus include a modified Atkins diet, a ketogenic diet, or a regular diet supplemented with triheptanoin (Pascual et al., 2014), the latter of which remains under investigation (clinical trial NCT03181399). Despite seizure amelioration in two-thirds of G1D individuals who tolerate a ketogenic diet, none of the treatments are fully effective (Hao et al., 2017). Further, the diet can prove detrimental for seizures in a small fraction of patients ($n = 5$ of 220 patients; J. M. Pascual, clinical observations). Thus, alternative or additional treatments are needed (Klepper et al., 2020).

This, and the desire to augment cellular glucose influx in dementia and to suppress it in cancer, provided the motivation to identify novel modulators of glucose transport. We therefore tested a series of compounds for effect on the accumulation of a glucose analog reporter in cultures of the pulmonary squamous adenocarcinoma cell line HCC95. These cells express Glut1 at about 10-fold greater abundance than all other glucose transporters combined (Goodwin et al., 2017b).

Numerous compounds exhibited glucose transport modulatory activity. However, prior information on Glut1- or glucose transport–relevant actions for most of them was lacking. Thus, instead of proceeding to characterize the compounds in mechanistic terms, we reasoned that their impact on the G1D mouse phenotype could constitute an expeditious and effective preliminary sorting criterion. To this end, we used the cited G1D mouse model, which harbors about 50% residual Glut1 activity, in line with human observations (Marin-Valencia et al., 2012). Importantly, G1D persons almost invariably exhibit motor dysfunction, and this is replicated by the mouse model. Thus, this mouse phenotype could constitute a robust test bed to evaluate the drugs. Because of ataxia, the G1D mice proved unsuitable for rotarod testing but could be evaluated by assessment of spontaneous locomotion via the measurement of body part spatial relations during motion. While measuring these relations for the first two drugs (acetazolamide and baclofen), we observed differential effects on various measures of gait, indicating that individual body part movements are not uniformly amenable to modulation. Thus, to facilitate and expand this analysis, we drew upon a machine learning assisted method that we previously developed for rotarod motor evaluation (Jakkamsetti et al., 2021) using deep learning

neural networks. This allowed for the identification of 49 locomotor parameters that differentiated G1D from control, which were differentially sensitive to treatment with saline as control or glucose as therapy. Altogether, the results of our screening and analysis method suggest that numerous prescription and other unsuspected drugs can exert glucose transport stimulation or inhibition and that locomotor testing in G1D mice is suitable for their sorting.

Materials and Methods

High-Throughput Screening

High-throughput screening (HTS) was performed at the High-Throughput Screening Shared Core at University of Texas (UT) Southwestern.

Chemical Libraries. We used the Prestwick Chemical Library (1200 compounds in clinical use), National Institutes of Health (NIH) Clinical Collection (446 compounds in clinical use or used in previous clinical trials), and the UT Southwestern Diversity Pilot Library (9967 compounds that are a diversity-based subset of the larger UT Southwestern Medical Center chemical library, which contains ~200,000 druglike compounds). The Diversity Pilot Library includes druglike molecules in accord with Lipinski's Rule of Five (Lipinski et al., 2001). All compound libraries were maintained in 100% dimethyl sulfoxide (DMSO) at $-20°$C.

HTS Assay. Glucose assay in cells employed a Glucose Uptake Cell-Based Assay Kit (catalog number 600470; Cayman, Inc.) essentially as described by the manufacturer using the non–small-cell lung cancer (NSCLC) cell HCC95 (Goodwin et al., 2017b). The assay was optimized for a 384-well-plate format as follows. HCC95 cells were plated at a final density of 8500 cells per well into 384-well plates (catalog number 781091; Greiner, Inc.) in 60 μl of growth medium (RPMI-1640 medium, catalog number A1049101; Fisher Scientific Inc.) plus 5% fetal bovine serum (catalog number S11150; Atlanta Biologicals, Inc.) and incubated overnight at 37°C (5% CO_2). The medium was then removed using an EL-406 plate washer (Agilent, Inc.), and the cells were washed once with phosphate-buffered saline. Glucose-free medium (55 μl) was added to each well using a MicroFlo dispenser (Agilent, Inc.). The library compounds were added at a final concentration of 2.5 μM to columns 3–22 of each assay plate with an Echo655 (Beckman-Coulter, Inc.). This concentration was informed by the inhibitory constant (Ki) of common Glut1 inhibitors (typically 1–10 μM) (Meyer et al., 2018). DMSO was added to columns 1, 2, and 23. Columns 2 and 23 served as vehicle control. The cells were then incubated for 24 hours at 37°C (5% CO_2).

Fluorescently labeled (2R,3R,4S,5R)-3,4,5,6-tetrahydroxy-2-((7-nitrobenzo[c][1,2,5]oxadiazol-4-yl)amino)hexanal (2-NBDG) (https://pubchem.ncbi.nlm.nih.gov/compound/2-nbdg) was used as reporter or surrogate of glucose transport. 2-NBDG was added to column 1 of each assay plate (as positive control) to a final concentration of 900 μM and 300 μM in columns 2–23. The concentration of 300 μM was selected based on the kit manufacturer's recommendation. Because positive controls of glucose uptake have not been described, a 3-fold greater concentration of 2-NBDG (900 μM) was used as a positive control. The final concentration of DMSO in all wells was 0.5%. After addition of 2-NBDG, assay plates were incubated for 20 hours at 37°C (5% CO_2). Afterward, the assay plates were centrifuged for 5 minutes at 400 g at room temperature, and the growth medium was exchanged for 100 μl of cell-based assay buffer with propidium iodide using an EL406 Plate Washer (Agilent, Inc.) following the manufacturer's instructions (Cayman, Inc.). Assay plates were then centrifuged at 400 g for 5 minutes at room temperature. The cell-based assay buffer was aspirated and replaced with 60 μl of cell-based assay buffer (without propidium iodide) using an EL406 plate washer and imaged on an INCell Analyzer 6000 (Molecular Devices, Inc.) for 2-NBDG (excitation/emission: 485/535 nm) and for
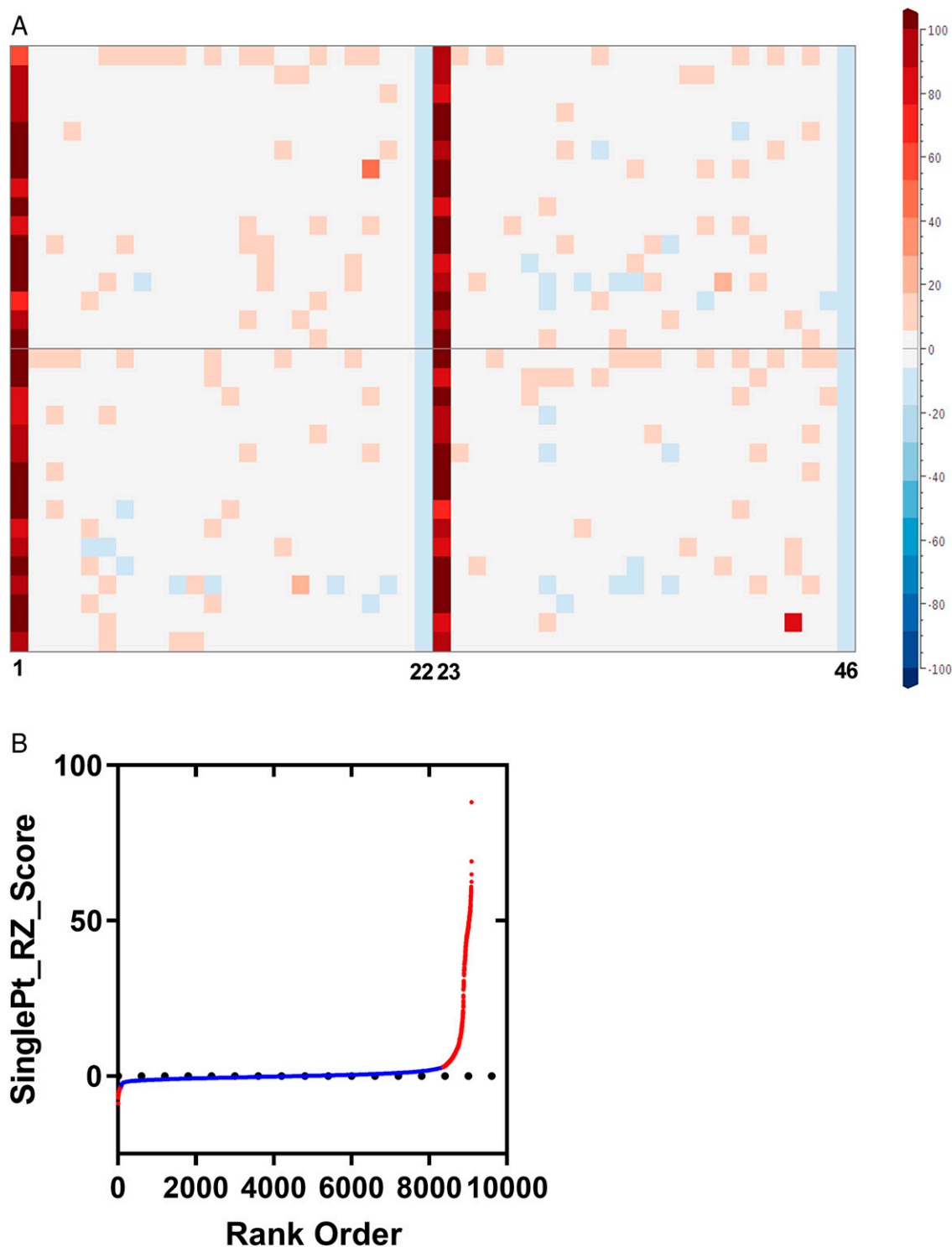
Fig. 1. High-throughput screening for modulators of glucose transport in HCC95 cells. (A) Heat map of activities observed in the primary screen with the US Food and Drug Administration (FDA)-approved drugs collection from Prestwick Chemical, Inc. The map was generated in the Analyzer module of the Screener software suite (version 16; Genedata, Inc.), where red, white, and blue wells indicate activities greater than, equal to, and less than, respectively, the robust mean of the library wells. The positive activities are presented in columns 1 and 23, and the DMSO activities are in columns 22 and 46 (as labeled under the image). (B) Quantile-quantile plot of screening results for the 8000-compound subset and the FDA-approved drugs collection. Robust Z scores (RZ scores) were calculated for each library compound and rank ordered from low to high. Red symbols indicate compounds with RZ scores >3 (activators) and <−3 (inhibitors).

propidium iodide–stained cells (excitation/emission: 488/650 nm). After excluding dead (i.e., propidium iodide–positive) cells from quantitation, the 2-NBDG signal was measured using CellProfiler (Jones et al., 2008) (Fig. 1).

Analysis of HTS Data. The Screener analysis suite (version 16; Genedata, Inc.) was used as described (Zhang et al., 2015). Compound activities were summarized as percent (%) effect relative to test population (compound library wells), and robust Z scores

(RZ scores) were calculated as previously (Wu et al., 2008). In brief, we used Genedata's Screener analysis suite to determine a robust mean (μ_p) and standard deviation (σ_p) for the test population (chemical library compounds) on each assay plate. We then determined the RZ score for each compound using the following equation:

$$RZ\ score = \frac{(x_{ijp} - \mu_p)}{\sigma_p} \qquad (1)$$

where x_{ijp} is the normalized activity x of the compound in row i and column j on plate p, μ_p is the robust mean of all compound wells on plate p, and σ_p is the robust standard deviation of all compound wells on plate p. An RZ score >3 or <-3 is scored as a statistically significant hit in the primary assay. Compounds with RZ scores >3 (activators) or <-3 (inhibitors) were marked as "primary hits" in the initial or primary screening. This is marked as primary screening in the Supplemental Material. Of note, there are no known Glut1 activators. Therefore, potency comparisons with established compounds were not feasible.

Confirmation of Primary Screening Hits. Compounds from the primary screen were individually taken from the chemical library and tested in the primary assay at the three doses (0.83, 2.5, and 7.5 μM) with three replicates per dose. Using the assay described above, we performed a confirmation study for each compound to determine if the activity observed in the primary screen (one dose, one replicate) was reproducible and dose responsive. We dosed each compound at 2.5 μM and two additional doses in the glucose uptake assay (a half log lower and a half log higher). We then summarized the activity of each compound at each dose by calculating the median activity from the normalized glucose update activities for the three replicates at each dose (relative to vehicle DMSO). Compounds that demonstrated activity at the screening dose and at least one additional dose were selected for further studies. In the Supplemental Material, this is considered the confirmatory screening. Of note, fluorescent compounds that overlapped the excitation and emission profile of 2-NBDG were excluded; this examination was carried out using the same assay without HCC95 cells (medium only).

Mouse Model

Mouse studies were carried out in accordance with the Guide for the Care and Use of Laboratory Animals as adopted the National Institutes of Health and were approved by the UT Southwestern Institutional Animal Care and Use Committee.

Wild-type (WT) C57BL/6J mice were purchased from the Jackson Laboratory. G1D mice were previously described (Marin-Valencia et al., 2012; Rajasekaran et al., 2022). These mice uniformly display frank ataxia with normal lifespan and other habits. They are also phenotypically superior, for this purpose, to our hemizygous mouse model (which is hypomorphic on several aspects) (Wang et al., 2006) or to other antisense DNA models (which harbor severe brain malformations) (Heilig et al., 2003). All of the mice were housed in humidity- and temperature-controlled facilities on a 12-hour on/12-hour off light/dark cycle with ad libitum access to food and water except as noted for testing. Estrous cycle was not considered.

Drug and Glucose Administration to Mice, Locomotor Testing Sequence, and Statistical Analysis

Habituation to the testing environment and locomotion recording were performed within the 9 a.m. to 5 p.m. period (i.e., in the light phase of the day cycle). Figure 3 and Fig. 4 illustrate the drug administration and testing sequence for acetazolamide and baclofen, respectively. The purpose of the mouse locomotor testing was not to perform dose-response calculations but to detect locomotor impact and thus enable drug selection for future characterization. Therefore, we aimed to maximize biologic impact by using doses and frequency of administration likely to be cumulative.

Acetazolamide. Twelve 9-month-old male G1D mice with a mean body weight of 23.27 g were used. Acetazolamide (product number A6011; Sigma-Aldrich, St. Louis, MO) was dissolved in saline. Dose (200 mg/kg) and route of administration (i.p.) were based on previous studies (Anderson et al., 1986; Czuczwar et al., 1986; Perles-Barbacaru et al., 2012; Szczygielski et al., 2019). On testing days, animals were habituated to the testing room for 1 hour inside their home cages. On testing day 1, 0.2 ml of saline was administered i.p. 30 minutes prior to locomotion testing. This was followed by a 1-hour rest interval in the home cage. Then, 200 mg/kg i.p. acetazolamide was administered three times at 2-hour intervals. Locomotion was again recorded 1 hour after the first and second administrations. The times of testing relative to injection were based on previous studies indicating that acetazolamide is detectable in the brain 1 hour after injection (Ichikawa et al., 1998) and that saline injection does not raise blood mouse glucose levels 30 minutes after injection (Zhao et al., 2017). On testing day 2, locomotion was recorded 24 hours after the first administration of acetazolamide the day before.

Baclofen. Seventeen 7-month-old male G1D mice with a mean body weight of 21.23 g were used. Baclofen (product number B5399; Sigma-Aldrich) was dissolved in saline. Doses (1.5 and 10 mg/kg) and route of administration (i.p.) followed previous studies (Cryan et al., 2004; Ebenezer and Prabhaker, 2007; Li et al., 2013; Varani et al., 2014). On testing days, animals were placed in the testing room for 1 hour for habituation prior to testing in their home cages. The route and times of saline and baclofen administration and testing were similar to acetazolamide except that the first and second doses of baclofen were 1.5 mg/kg and the third dose was 10 mg/kg.

Glucose. Ten control (five females and five males) and 10 G1D (five females and five males) mice aged 5 months were used. The mice were fasted for 5 hours prior to the first injection. On testing day 1, locomotion was recorded without the administration of saline or glucose (product number G8270; Sigma-Aldrich). On day 2, which was the following day, locomotion was recorded 30 minutes after 0.2 ml i.p. saline injection. On testing day 3, which was five days later, locomotion was recorded 30 minutes after i.p. glucose injection at 2 g/kg of body weight using a 0.25-g/ml glucose solution in saline. Five-microliter blood samples were collected from mouse tail clips immediately after locomotion recording, and glucose concentration was determined with a Contour glucometer (Bayer, Tarrytown, NY).

A paired t test was used within each drug experimental group to examine the differences between saline and the subsequent postdrug (acetazolamide or baclofen) locomotion sessions. For the glucose experiments, the control mouse group was compared with the G1D group at baseline using an unpaired two-sample t test, whereas a paired sample t test was performed to compare the effects of saline and glucose injections between the control and G1D groups.
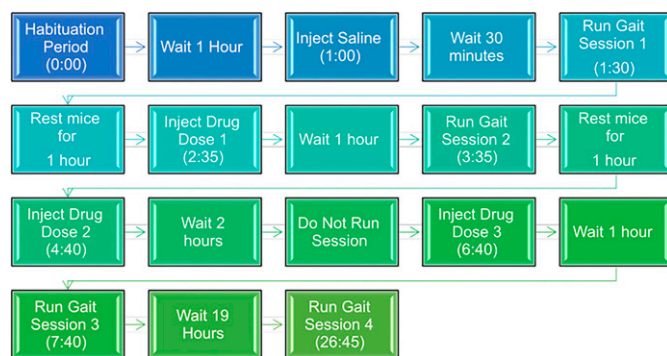
Mouse Locomotion Analysis

Mice were daily assessed for appearance and general health prior to locomotor testing. An illuminated, five-track rodent runway platform with plexiglass-separated lanes (Fig. 2) was built to allow the video recording of the undersides of the mice through a glass platform. This enabled the tracking of predetermined key points of each mouse body while it traversed the runway. The mice were untrained. Occasionally, some mice were prodded with a blunt object to facilitate the crossing of the entire platform. These events were not removed from analysis. Drug doses for mouse studies were estimated from published data on dose and half-life. We defined a testing session as a set of three trials. During a trial, a mouse crossed the track for one dose of experimental drug, saline, or no intervention. A trial was typically completed without stopping for more than 10 seconds.
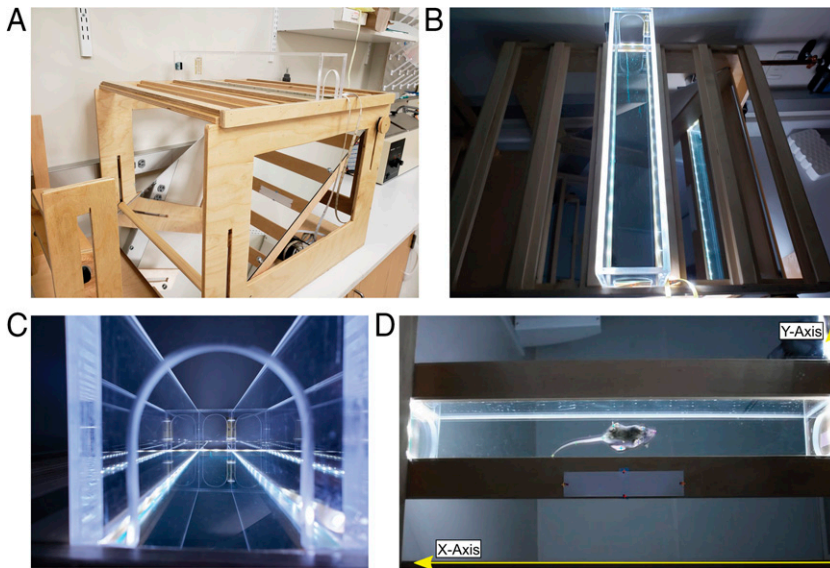
Fig. 2. Locomotor testing platform. (A) Custom designed mouse track apparatus. (B and C) Illumination by light emitting diodes is shown for the middle lane of the track apparatus. This configuration enabled a more precise detection of mice body parts. (D) Example labeled frame from the recorded videos. The colored + signs on the plot represent manual annotations used for training the network. Four points are marked on the track (white box) and used as a length calibration for post hoc analysis.

Video Acquisition and Preprocessing

Bottom (i.e., from below the locomotion plane) view videos of the mice were recorded using a Nikon D7200-N1406 digital SLR camera with an 18–140 mm lens placed parallel to the platform. The videos were recorded at 30 frames per second (fps) with a resolution of 1920 × 1080 pixels for acetazolamide and baclofen recordings and 60 fps for all subsequent recordings. This difference in video recording temporal resolution was due to the fact that recordings at 30 fps were sufficient to measure the locomotor behavior of the mice after acetazolamide and baclofen using Kinovea (version 0.9.3; https://www.kinovea.org) while allowing for a favorable data analysis time. For subsequent glucose experiments, we implemented the fully automated deep neural network-based pose estimation package DeepLabCut (Mathis et al., 2018; Nath et al., 2019). Although the DeepLabCut network was trained adequately, some points recorded at 30 fps were mislabeled because of the fragmented nature of G1D mice and body part relations in the recorded videos. Increasing the frame rate of the camera from 30 fps to 60 fps allowed for adequate automatic extraction of pose activity from G1D mouse videos. Optimum image resolution required for accurate and expedient training of neural networks was 1280 × 720 pixels. Therefore, preprocessing adjusted the videos to this resolution using a Microsoft video editor.

Locomotion Analysis of Acetazolamide and Baclofen

Acetazolamide (200 mg/kg) was injected i.p. into 12 G1D male mice that were 7 or 9 months of age. Four sessions were conducted with the first after a saline injection to control for the subsequent three sessions (Fig. 3). The interval between injection and testing was 30 minutes for saline and 1 hour for acetazolamide. Two hours after the first session was completed, each of the three subsequent sessions was conducted after a dose of the drug with an interval of 1 hour between sessions and doses. Baclofen was tested using 18 G1D male mice 7 months old after a 1.5-mg/kg i.p. dose. Three sessions included saline control, followed by two more sessions (Fig. 4). Two hours after the first session was completed, each of the two other sessions was conducted after a dose of the drug with an interval of 2 hours between sessions and doses. We also tested a second dose (10 mg/kg) in a subsequent session that followed the last session by 3 hours. Videos recorded during these trials were used to track the hind limbs of the mice using semiautomated annotation software Kinovea.

These drugs caused visible changes in locomotion. To evaluate their effects, pose-estimation coordinates of hind limbs were imported to MATLAB. The speed was calculated using function 'diff' by dividing the displacement by the time between any two video time frames.
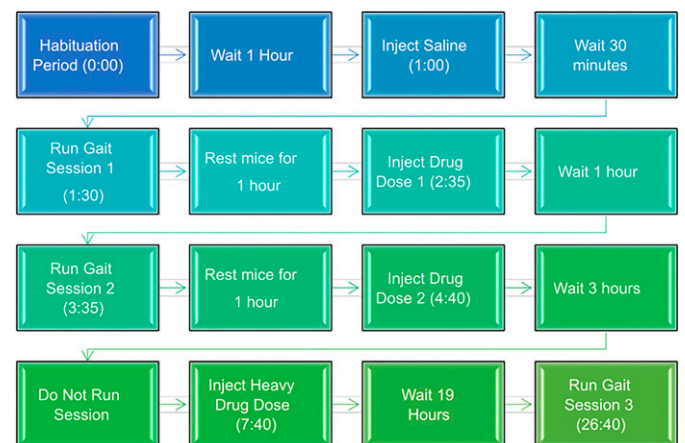

Fig. 3. Diagram of mouse acetazolamide injection studies. Schedule of events used for the testing of acetazolamide effects on G1D and control (WT) mice. Every other block in the diagram indicates how much time has elapsed along with what action is performed at that point in the timeline. Since each mouse takes an average of 5 minutes to complete each locomotor session, 5 minutes are added to the total time elapsed going forward in the timeline. Injection times per mouse are excluded from the total elapsed time since injections take less than a minute to administer and are thus negligible.

Fig. 4. Diagram of mouse baclofen injection studies. Schedule followed for testing baclofen on G1D and control (WT) mice. The timeline for the baclofen drug is similar to that of acetazolamide (Fig. 3) except that the third injection and subsequent locomotor session are replaced with a longer pause before the second dose followed by a larger overnight dose.

MATLAB 'pdist' function was used to obtain the Euclidean distance between the hind paws (i.e., gait width). The stationary gait width was calculated within the first 500 milliseconds of mouse placement on the track, with the stationary period defined as lack of any movement velocity greater than 5 cm/s. Subsequently, moving gait width and speed were similarly computed for movement speeds above 5 cm/s. Stride was evaluated using a speed versus the x-coordinate graph of the limb. In this manner, multiple speeds were detected. The area between a speed value below zero and the next consecutive value below zero represented one swing motion. The distance between two consecutive minimum speeds was defined as the stride length, whereas the average swing speed was calculated by averaging the speed values between two consecutive minimum speed values. These seven parameters sufficed to statistically determine significant changes induced by the drugs.

Automation of Pose Estimation by Deep Neural Networks

The semiautomated testing of acetazolamide and baclofen described above was sufficient with only the two hind limbs tracked, as the changes in locomotion were salient. However, we expanded the tracking to multiple body parts to analyze more subtle changes that the drugs may potentially cause. Because of the ataxic locomotion of G1D mice, multipoint tracking of mouse body parts proved imprecise using Kinovea (Shishov et al., 2021). Thus, we used a deep neural network for completely automated pose estimation.

DeepLabCut 2.2.0.2 was used for automated tracking of body parts in the recorded videos. This was tested for no injection and for saline and glucose administrations. Ten G1D mice and 10 littermate control mice 7 months old with half of each group comprising males were tested in three sessions: baseline, saline, and glucose administrations. To propitiate metabolic homogeneity, the mice fasted from 9:30 a.m.

to 2:30 p.m. for all three sessions. Blood glucose was measured using a Contour Next EZ glucometer. Baseline sessions were conducted the day before saline, and glucose sessions were performed five days later. Saline injection volume was 0.2 ml for all mice. Glucose dose was 2 mg/g dissolved in the same volume. Injections were followed by a 15-minute pause before placement on the track.

Deep Learning Neural Network Tracking Dataset. From 60 videos (three sessions including 20 mice), the six videos that displayed the most diversity with respect to mouse behavior and lighting were selected for training. Five additional videos with different camera angle and zoom settings were also selected. Using a k-means algorithm, 350 frames were selected from these 11 videos. On these frames, 12 points were manually labeled with precision, with eight body parts on each mouse and four points on the track for calibration (Fig. 5A).

Network Training and Performance Evaluation. The training dataset was created using the ImageNet pretrained ResNet-50 architecture (Mathis et al., 2020). To mitigate motion blur, an 'imgaug' method was chosen for data augmentation. The training was performed using 95% of the annotated frames, whereas 5% of the frames were used for evaluating the network. The evaluation was accessed after 500,000 iterations to determine the best fit model. The final model was created using 1.03 million iterations, which had a combined train error of 1.48 pixels and a test error of 9.31 pixels for all labeled parts.

Tracking of Novel Videos. Using the trained model, all of the recorded videos—54 novel and the six used for training—were analyzed. The results were saved in Excel. Labeled videos were created to verify the performance of the network for both control and G1D mice. The purpose was to relabel any outlier frames and add to the training dataset any outlier frames for retraining the network. However, the prediction on the final labeled videos was satisfactory, and the model was therefore not retrained.

Fig. 5. Locomotor effects of glucose injections. (A) Picture taken from video illustrating body parts and calibration points that were tracked by DeepLabCut. (B) Example PCA plot generated using the feature set of 49 behavioral parameters shows the separation between the two cohorts of mice at baseline. Control (WT) and G1D mice are represented by red and blue, respectively. (C) Parameters that displayed statistical significance for the G1D group after glucose injections. The top row illustrates average speed and rate of change of speed of left hind limb and of tail base (left to right) for G1D mice. The bottom row displays average speed and rate of change of speed of left hind limb and of tail base (left to right) of control mice. Paired t test with α = 0.05 was performed on these comparisons (* and ** stand for $P < 0.05$ and $P \leq 0.01$, respectively).
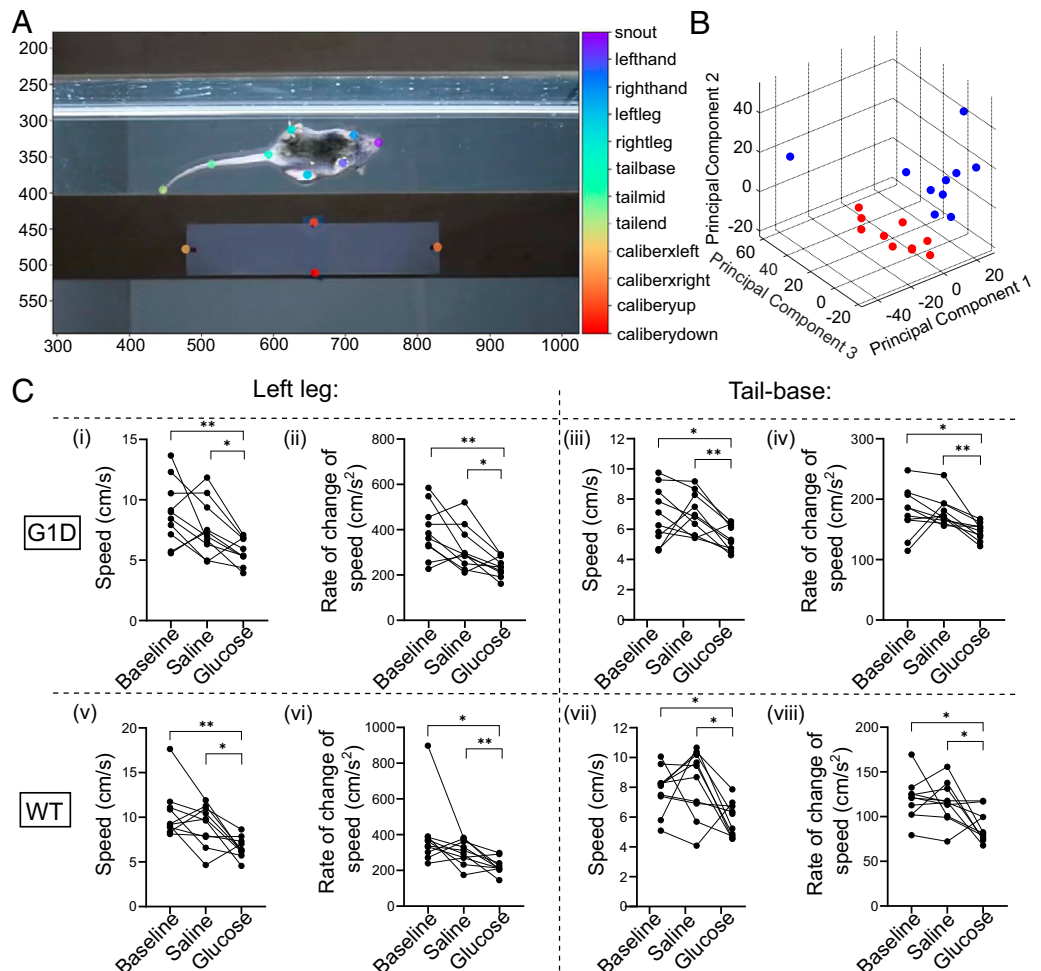
TABLE 1
Evaluation of error test rates using DeepLabCut
Errors were obtained after evaluating the trained DeepLabCut network with multiple p-cutoff values. Error values were calculated as the distance (in pixels) between the labels marked by DeepLabCut network and the scorer. The results displayed here were generated using p-cutoff (likelihood) ranging from 0.09 to 0.9. These values were then used to determine the appropriate p-cutoff value for thresholding.

P-Cutoff Used	Train Error with P-Cutoff	Test Error with P-Cutoff
0.09	1.2	3.84
0.1	1.2	3.84
0.2	1.2	3.84
0.3	1.2	3.37
0.4	1.2	3.37
0.5	1.2	3.37
0.6	1.2	3.33
0.7	1.2	3.33
0.8	1.2	3.31
0.9	1.2	3.17

Preprocessing and Data Optimization. The Excel datasheets were imported into MATLAB. Each labeled mouse part contained three values: x-coordinate in pixels, y-coordinate in pixels, and the likelihood of the prediction being accurate. Euclidian pixel distance values were converted to centimeters using four points marking the track for calibration. Even while displaying a low error rate, the network did detect rare outliers in several frames. For instance, the paws of the animals were not touching the plexiglass while being placed on the platform (first few seconds). Therefore, we set a low threshold for likelihood and then filtered and interpolated the data to facilitate automated tracking. A low-likelihood threshold (p-cutoff) was selected to include all of the high-confidence and the majority of low-confidence data points. The low-confidence points were included to not have gaps in

tracking values, and any outliers would later be removed during preprocessing. A low likelihood threshold of 0.09 (9% likelihood) was selected after inspecting the evaluation test error rate (Table 1). A histogram with a nonparametric kernel-smoothing distribution was generated for the y-coordinate values using the MATLAB 'histfit' function (Fig. 6C). All values beyond certain lower and upper threshold limits in the histogram, which were set using the normal range of motion possible on the track, were discarded and the final data were interpolated using the 'interpl' function (Fig. 6, A and B).

Behavioral Profiling Parameters. A total of 49 locomotor measures were extracted from the selected data (Table 2). These measures were based on both stationary and movement parameters of the mice. Parameters were calculated for the first forward motion on the track (half lap), one stationary period, and the entire duration on the track. The first half lap on the track and one stationary period were extracted manually using the function 'ginput' in MATLAB. The body parts analyzed, the duration for which the feature was extracted, and the nature of the feature (temporal/spatial) are in Table 2. The definitions of the features are in Table 3.

Statistical Analysis

Statistical tests employed MATLAB R2021a and GraphPad Prism 9. Two-sample t tests (MATLAB's 'ttest2') were used to calculate control relative to G1D group differences. Student's paired t test (MATLAB 'ttest') was used to compare changes due to saline and glucose injections within each group. $P < 0.05$ was considered statistically significant.

Principal Component Analysis

To visualize differences between different trials and groups, cluster analysis was performed using MATLAB principal component analysis algorithm 'pca'. All 49 parameters described above (Table 2) constituted the feature set for pca, which was used to compare
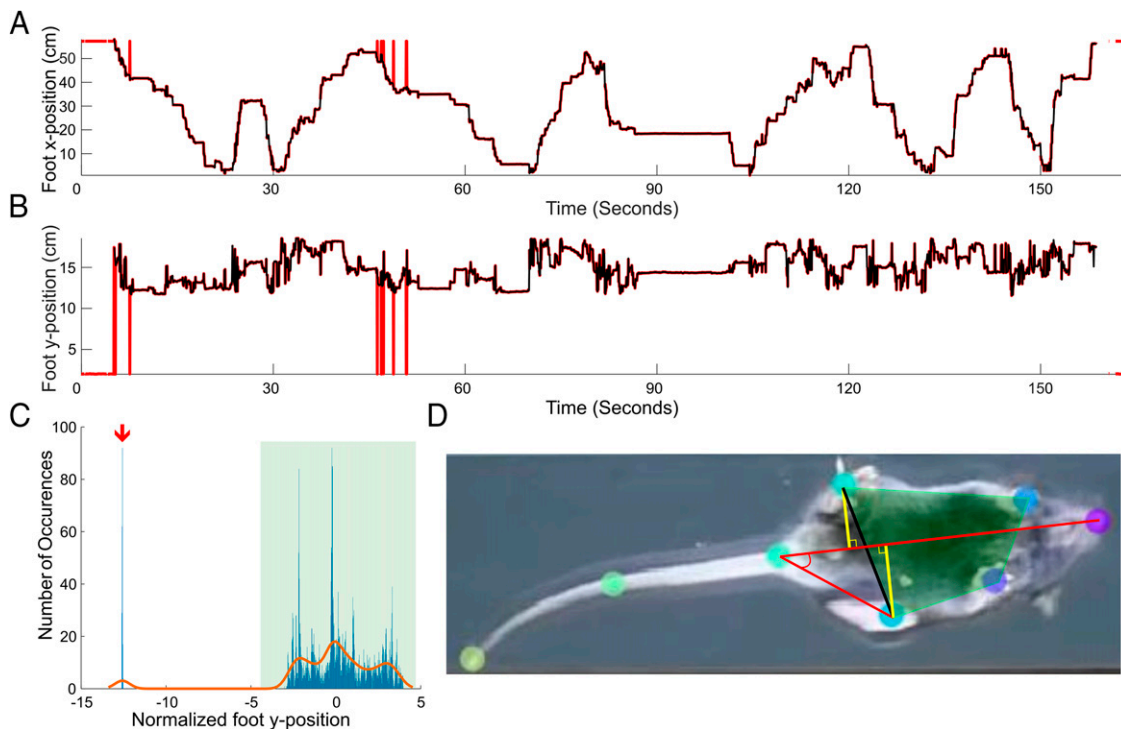
Fig. 6. Locomotor data preprocessing. (A and B) X- and y-coordinate data of left hind limb before preprocessing (red) and after preprocessing (black). (C) Output of the MATLAB's 'histfit' function with kernel-smoothing distribution used for preprocessing poses estimation data. After appropriate thresholding, the representative green shaded box region was retained, which helped remove outliers (outlier peak is highlighted by a red downward facing arrow). (D) Example spatial parameters that were generated. Angle between two red lines (snout to tail base and tail base to left hind limb) was recorded as stride angle. The black line separating the hind limb represents the hind limb width, whereas the hind limb separation from the body was calculated as the sum of two perpendicular yellow lines. The green shaded polygon represents the mean limb area.

TABLE 2
Locomotor parameters that characterize mouse gait
These 49 features were calculated from the pose coordinates of the mice placed on the testing platform track. Every feature is associated with the body parts analyzed and the duration on the track for which it was calculated. The 49 features segregate into 31 temporal and 18 spatial features.

Number	Feature	Body Part Analyzed	Duration on Track	Feature Type
1	Mean speed	Left hind limb	All laps	Temporal
2	Median speed	Left hind limb	All laps	Temporal
3	Mean speed	Left hind limb	Half lap	Temporal
4	Median speed	Left hind limb	Half lap	Temporal
5	Mean speed	Tail base	All laps	Temporal
6	Median speed	Tail base	All laps	Temporal
7	Mean speed	Tail base	Half lap	Temporal
8	Median speed	Tail base	Half lap	Temporal
9	Mean rate of change of speed	Left hind limb	All laps	Temporal
10	Median rate of change of speed	Left hind limb	All laps	Temporal
11	Mean rate of change of speed	Left hind limb	Half lap	Temporal
12	Median rate of change of speed	Left hind limb	Half lap	Temporal
13	Mean rate of change of speed	Tail base	All laps	Temporal
14	Median rate of change of speed	Tail base	All laps	Temporal
15	Mean rate of change of speed	Tail base	Half lap	Temporal
16	Median rate of change of speed	Tail base	Half lap	Temporal
17	Mean forward speed smoothness	Left hind limb	All laps	Temporal
18	Mean forward speed smoothness	Left hind limb	Half lap	Temporal
19	Mean lateral speed smoothness	Left hind limb	All laps	Temporal
20	Mean lateral speed smoothness	Left hind limb	Half lap	Temporal
21	Mean forward speed smoothness	Left hind limb	Stationary period	Temporal
22	Mean lateral speed smoothness	Left hind limb	Stationary period	Temporal
23	Mean forward speed smoothness	Tail base	All laps	Temporal
24	Mean forward speed smoothness	Tail base	Half lap	Temporal
25	Mean lateral speed smoothness	Tail base	All laps	Temporal
26	Mean lateral speed smoothness	Tail base	Half lap	Temporal
27	Half lap time	Left hind limb	Half lap	Temporal
28	Number of jerks	Left hind limb	Half lap	Temporal
29	Maximum stride speed	Left hind limb	Half lap	Temporal
30	Mean stride speed	Left hind limb	Half lap	Temporal
31	Stride speed variation	Left hind limb	Half lap	Temporal
32	Mean stride angle	Left hind limb and axis of the body	Half lap	Spatial
33	Median stride angle	Left hind limb and axis of the body	Half lap	Spatial
34	Mean hind-limb width	Both hind limbs	Half lap	Spatial
35	Median hind-limb width	Both hind limbs	Half lap	Spatial
36	Mean hind-limb width	Both hind limbs	Stationary period	Spatial
37	Median hind-limb width	Both hind limbs	Stationary period	Spatial
38	Mean hind limb separation from the body	Both hind limbs and axis of the body	Half lap	Spatial
39	Median hind limb separation from the body	Both hind limbs and axis of the body	Half lap	Spatial
40	Mean hind limb separation from the body	Both hind limbs and axis of the body	Stationary period	Spatial
41	Median hind limb separation from the body	Both hind limbs and axis of the body	Stationary period	Spatial
42	Mean limb area	All four limbs	Half lap	Spatial
43	Median limb area	All four limbs	Half lap	Spatial
44	Mean limb area	All four limbs	Stationary period	Spatial
45	Median limb area	All four limbs	Stationary period	Spatial
46	Mean stride length	Left hind limb	Half lap	Spatial
47	Maximum stride length	Left hind limb	Half lap	Spatial
48	Mean stride length	Left hind limb	Half lap	Spatial
49	Stride length variation	Left hind limb	Half lap	Spatial

baseline with saline, saline with glucose, and baseline with glucose for both groups of mice. Linear discriminant analysis (LDA) was implemented on the principal component values to determine the components that displayed maximum class separation. To evaluate this classification, a confusion chart was generated for observing the true labels and predicted labels. Subsequently, one-way multivariate analysis of variance ('manova1' in MATLAB) was performed on the principal components to determine the statistical significance of the group mean classification. This statistical model provided a robust method for quantifying the cluster separation.

Results

High-Throughput Screening

Our adaption of a commercial protocol (Cayman, Inc.) from a 96-well assay format to a 384-well format proved suitable for HTS. The optimal HCC95 cell number per well was 8500, and the incubation times for glucose starvation and 2-NBDG were optimized to 24 and 20 hours, respectively, which maximized the assay time window. For positive control (e.g., increased uptake of 2-NBDG), we used a 2-fold higher concentration of 2-NBDG compared with DMSO control wells and the wells where the chemical library was added (columns 3–22). The assay was unaffected by DMSO concentrations up to 0.5%. Automated media exchange further afforded Z′ factors of ~0.62, thus indicating HTS assay robustness (Zhang et al., 1999).

Figure 1 illustrates typical plate results obtained from the screening of a clinical/preclinical drugs collection (Prestwick Chemical Libraries and NIH Clinical Collection) and a diversity-based pilot library of 9967 druglike small molecules. Compounds from both libraries were scored for activity (% effect relative to control and RZ score; see methods and Fig. 1). Ten glucose transport activators were confirmed from the approved

TABLE 3
Description of the movement parameters
The movement features cited in Table 2 are defined in this table.

Feature	Definition of Feature
Speed	Magnitude of the difference in the position of the limb/paw between two successive frames divided by the interframe duration. Mean and median speeds were calculated for both x- and y-coordinates for all cited motion types.
Rate of Change of Speed	Difference in the instantaneous speed between two successive frames divided by the interframe duration.
Speed Smoothness/Spectral Arc Length	Smoothness of speed of a limb using MATLAB's 'fft' function (Jakkamsetti et al., 2021).
Stride Angle	Angle of the limb calculated from the axis of the body at the end of a forward stride. This can estimate if the stance is narrow or wide.
Hind Limb Width	Euclidean distance between the hind limbs of the mouse.
Hind Limb Separation from Body	Perpendicular distance of the hind-limb paws from the axis of the body (snout to tail base).
Limb Area	Area of the polygon subtended by all four limbs of the mouse.
Half Lap Time	Time spent by the mouse in completing a half a track (one forward motion) (i.e., one length of the track).
Number of Jerks	Sudden increases in the speed of the limb during the first half track movement were recorded. This parameter is the total number of such jerks during one forward motion.
Stride Length	Distance between two consecutive minimum speed values (would mean that the limb is in contact with the surface) on speed vs. x-coordinate (distance) graph of left foot. It was calculated for one forward motion (half a track), similar to acetazolamide and baclofen methods.
Stride Speed	Minimum speed in speed vs. distance graph were further evaluated. Average of speed values between two consecutive minimum speed values was recorded as stride speed.

or preclinical drugs (Supplemental Excel File 1), and 32 additional activators were identified from the diversity-based pilot library. Supplemental Table 1 includes a summary of the uses and other information available for the approved or preclinical drugs. Of these 42 activators, 37 were compounds not previously described in Glut1 or glucose transport–related studies. Two inhibitors were identified from the approved/preclinical drugs and seven from the diversity-based pilot library. None of the nine inhibitors have been previously described in Glut1-related studies. Four compounds that were positive in an initial screen were not further pursued because of fluorescence (verteporfin, metformin, pyrvinium pamoate, and auranofin).

These results are summarized in Table 4 and provided in full in Supplemental Tables 1–8. These tables divide the results into primary and confirmatory screening results. Specifically, Supplemental Table 1 presents salient literature on top Prestwick-NIH glucose transport activators relevant to Glut1-related aspects, Supplemental Table 2 lists 91 NIH-Prestwick activators from the initial screening, Supplemental Table 3 lists six NIH and Prestwick inhibitors identified in the initial screening, Supplemental Table 4 lists 30 NIH and Prestwick activators and inhibitors that proceeded to dose response and autofluorescence confirmation, Supplemental Table 5 lists six NIH and Prestwick activators without autofluorescence and confirmation at all three doses, Supplemental Table 6 indicates four NIH-Prestwick activators without autofluorescence and confirmation at two doses, Supplemental Table 7 lists 8K

diversity screen activators and inhibitors, and Supplemental Table 8 lists seven inhibitors confirmed from the 8K diversity library. Supplemental Excel Files 1–7 give the chemical structures, Z scores, and catalog numbers for the activator and inhibitor compounds. Specifically, Supplemental Excel File 1 lists primary screening activator results for Prestwick and NIH libraries, Supplemental Excel File 2 lists primary screening inhibitor results for Prestwick and NIH libraries, Supplemental Excel File 3 lists confirmatory screening activator and inhibitor results for Prestwick and NIH libraries, Supplemental Excel File 4 lists primary screening activator results for the 8K diversity library, Supplemental Excel File 5 lists primary screening inhibitor results for the 8K diversity library, Supplemental Excel File 6 lists confirmatory screening activator results for the 8K diversity library, and Supplemental Excel File 7 lists confirmatory screening inhibitor results for the 8K diversity library.

Initial Testing of Drug Effects on Locomotion

To test behavioral effects, two activators were injected into mice. Figure 7 demonstrates the effect of acetazolamide and baclofen on the gait of G1D mice. Gait parameters after 1 hour and 5 hours of first acetazolamide injections were compared with saline injections. Stationary gait width increased significantly after 1 hour ($P < 0.001$; Fig. 7A) and after 5 hours of injecting the first dose ($P < 0.05$; Fig. 7B). These effects were reversible 24 hours after injection (not shown). We also assessed the effects of baclofen injections at different points

TABLE 4
Numbers of activators and inhibitors of glucose transport identified in HCC95 cells via high-throughput screening

Library	Compounds Screened	Activators		Inhibitors	
		Confirmed	Novel[b]	Confirmed	Novel[b]
Prestwick Chemical	1200	8	4	1	1
NIH Clinical Collection	446	2	1	1	1
UT Southwestern Diversity Pilot[a]	8000	32	32	7	7
Total	9646	42	37	9	9

[a]Representative of ~200,000 compounds.
[b]Confirmed compounds that have not been previously described in association with Glut1 or glucose transport.

Fig. 7. Locomotor effects of acetazolamide and baclofen. (A) Effect of acetazolamide 1 hour after injection. Stationary gait increases with high significance. (B) Stationary gait width after 5 hours of acetazolamide is higher than at saline after 5 hours of first injection. (C and D) Effect of baclofen 1 hour after injection. Stride length significantly decreases after 1 hour of administration. Average swing speed decreases with near significance. (*, **, and *** stand for $P < 0.05$, $P \leq 0.01$, and $P \leq 0.001$, respectively.)
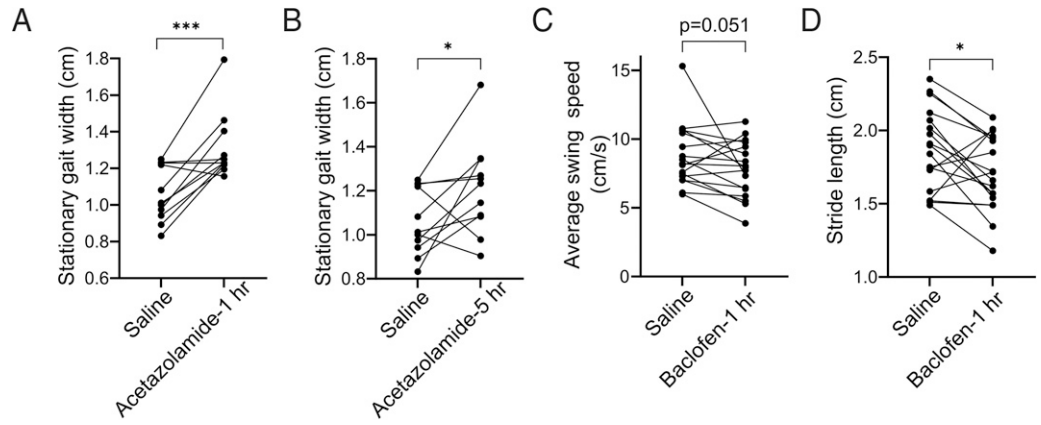
compared with saline injections. Several parameters demonstrated a significant change (Fig. 7, C and D). Average swing speed of the paw displayed changes that were close to attaining significance ($P = 0.051$; Fig. 7C). We also observed that stride length decreased significantly 1 hour after baclofen compared with saline ($P < 0.05$; Fig. 7D).

In-Depth Determination of Locomotor Parameters That Differentiate G1D from Control Mice

Because of the inhomogeneity in the significance of the baclofen results (Fig. 7, C and D) and to expedite the testing of the drugs [i.e., analyzing one drug dose consumed about 3 hours in the manual analysis of a group of five mice using the Kinovea video annotation tool (version 0.9.3)], we extracted a larger number of features from the videos using deep learning neural network tracking. The resulting expediency also eliminated potential bias implicit in the manual analysis of the results while improving the quality and reliability of the data being recorded.

Of 49 features identified via deep neural network analysis, 27 (55%) proved statistically significant (Student's t test, $\alpha = 0.05$) for differentiating G1D from control mice (Tables 2 and 3). Principal component analysis (PCA) revealed a clear separation between the two populations (Fig. 5B). Principal components 1, 2, and 3 together explained 61.7% of the total variation between the control and G1D groups. The parameter of half lap time exerted the most influence on principal component 1, whereas mean tail base rate of change of speed for one lap was the largest contributor to the variation in principal component 2. In principal component 3, the greatest influence was mean speed of tail base for the entire duration on the track. This indicated that most of the variation between the control and G1D mice was due to temporal (i.e., movement) parameters of these mice. The

time required to prepare a dataset and train the DeepLabCut network for 1.03 million iterations was approximately 48 hours. Once the network was trained to produce satisfactory tracking, it was used to extract pose from 20 mice for three trials. Extracting pose from one mouse video took approximately 7 minutes without any human intervention.

Saline and Glucose Effects

These parameters allowed us to test the effects of saline or glucose administration on locomotion. Saline injections were associated with increased blood glucose concentrations compared with baseline trials in G1D mice (Fig. 8). This was not observed in control mice. We detected a significant increase in blood glucose concentration after glucose injections in both groups. In G1D mice, measures of average speed of left hind limb, average rate of speed of left hind limb, average speed of tail base, and average rate of speed of tail base for the entire duration on the track demonstrated a significant change for saline relative to glucose and baseline relative to glucose (Fig. 5). These parameters were also different for control mice, albeit at a different level of statistical significance.

We also used the feature set of 49 parameters to perform PCA and determine the greatest cluster separation using linear discriminant analysis (LDA). As described in the methods, we performed multivariate analysis of variance (MANOVA) on these LDAs for all comparisons among baseline, saline, and glucose measurements. The results, shown in Table 5, for all seven comparisons were significant for d = 1, which enabled us to reliably reject the null hypothesis that the means of each group in the comparison were the same and that any difference observed in the sample set was due to random chance.

Fig. 8. Glucose levels and weights during glucose locomotor testing. Blood glucose levels of G1D mice (A) and control (WT) mice (B) of various weights measured after each session on the locomotor track. The blood glucose level of each mouse was measured at baseline on the first day (blue data points), followed by a saline injection on the second day (red), and finally with a glucose injection on the third testing day (green). Males and females are represented by triangles and dots, respectively.
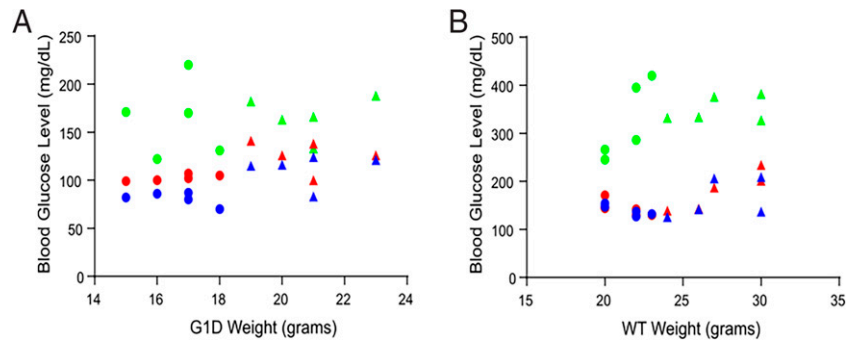
TABLE 5
Multivariate analysis of variance on baseline, saline, and glucose injection effects

MANOVA was performed on the principal component analysis values exhibiting the greatest cluster separation to compare the sample means. The d value for all of the MANOVA comparisons was 1, and associated P values are given in the table. D = 1 stands for rejecting the null hypothesis that the sample means are the same vector, but there is not enough evidence to reject that they lie on the same line. Control indicates normal littermate mice.

Group 1	Group 2	MANOVA P Value
G1D Baseline	Control Baseline	2.62E-08
G1D Baseline	G1D Saline	0.0052
G1D Saline	G1D Glucose	2.87E-04
G1D Baseline	G1D Glucose	7.87E-04
Control Baseline	Control Saline	4.05E-04
Control Saline	Control Glucose	2.42E-04
Control Baseline	Control Glucose	0.0044

Sex and Body Weight Effects

Because control and G1D mice exhibited different glucose level responses to saline injection, we investigated factors that may impact this response. Thus, we elucidated the effect of sex on mouse weight and blood glucose levels and further characterized saline effects on blood glucose in control relative to G1D mice by comparing the body weights of the 10 control and 10 G1D mice used in saline and glucose studies. As previously noted, (Marin-Valencia et al., 2012), G1D mice weighed less than control. The body weight of control and G1D mice was 24.30 ± 1.17 g and 18.40 ± 0.91 g, respectively (mean ± S.E.M., $n = 10$, $P < 0.01$). This difference was accentuated for G1D females relative to G1D males (Supplemental Fig. 1). Blood glucose concentration was greater in male G1D mice at baseline and after saline injections, but no difference was noted in control mice (Supplemental Fig. 2, A and B). Blood glucose level at baseline and after saline injection in G1D female mice was 81.00 ± 3.03 mg/dl and 102 ± 1.50 mg/dl, respectively (mean ± S.E.M., $n = 5$, $P < 0.01$). The same level in male G1D mice at baseline and after saline injection was 111.8 ± 7.39 mg/dl and 126.2 ± 7.22 mg/dl ($n = 5$, $P < 0.05$). We also examined the sex differences in locomotion in G1D mice at baseline and after saline injections for the four motor parameters that were presented in Fig. 5. Male and females were significantly different in speed and rate of change of speed only at baseline (Supplemental Fig. 2C) but not after saline injections (Supplemental Fig. 2D).

Discussion

We evaluated accumulation of the glucose analog 2-NBDG in HCC95 cells because they express Glut1 at greater abundance than other glucose transporters (Goodwin et al., 2017b). Glut1 in these cells is functional in the plasma membrane, as its expression is driven by aberrant phosphoinositide 3-kinase (PI3K)-mediated translational stabilization of hypoxia-inducible factor (HIF)-1α. These properties enabled us to attribute changes in the accumulation of the reporter to Glut1 mediated transport and/or to other unknown mechanisms. In contrast with 5TGM1 myeloma cells (D'Souza et al., 2022), L929 fibroblasts (Hamilton et al., 2021), or T cells (Sinclair et al., 2020), where 2-NBDG or 2-deoxyglucose entry measured over 4 to 60 minutes is mediated or complemented by Glut1-independent mechanisms, 2-NBDG enters (and exits) HCC95 cells via Glut1 (Goodwin et al., 2017a). The dominant facilitation by

Glut1 of native glucose transport, and the mechanism that enables this facilitation, is more robustly substantiated for HCC95 than for most other cell types by studies of its related in vivo tumors and xenografts using ^{18}Fluoro-2-deoxy-glucose, 2-deoxy-D-glucose, and the Glut1 inhibitor WZB117 (Goodwin et al., 2017a). HCC95 Glut1 levels are modulable and biologically impactful. For example, changes in expression of Glut1 by this cancer cell are relevant beyond glucose transport, as expression level is associated with glycolysis, tumor growth and patient death rates (Goodwin et al., 2017b). Thus, the exposure of HCC95 cells to the 2-NBDG reporter allowed us, in the context of control assays used for comparison, to identify in an unbiased manner activator and inhibitor compounds previously unknown or understudied in relation to Glut1 or glucose transport.

Only modest glucose transport increases such as those experienced postprandially are beneficial to G1D patients (von Moers et al., 2002; Akman et al., 2010; Koy et al., 2011; Parolin et al., 2011; Rajasekaran et al., 2022). This suggests that relatively small (i.e., below 2-fold) changes in net glucose transport can significantly ameliorate brain dysfunction in G1D. Thus, for any drug(s) to be potentially clinically useful, only a relatively modest increase on glucose transport activity may suffice. In contrast, excessive transport augmentation may be undesirable as illustrated by toxic Glut1 gain of function with consequent overstimulation of glycolysis (Allaman et al., 2015). This contention made us defer studying alternative approaches characterized by more vigorous or poorly regulable gain of function such as gene therapy as currently conceived.

Among the Prestwick and NIH Clinical Collection compounds, 10 are activators and two are inhibitors of glucose transport. Among the former are nine drugs used in disorders unrelated to glucose metabolism. The remaining activating drug (vanoxerine or GBR 12909 dihydrochloride), which is not approved for clinical use, has been studied in humans but is toxic. Most of these drugs are available in oral formulations. Only four have been used in neurologic diseases (acetazolamide, baclofen, vanoxerine, and idebenone). One compound has limited data for systemic bioavailability and is used topically (clotrimazole). Some of these transport activating drugs (hesperidin, itraconazole, and telmisartan) have been studied in cell line or animal models for Glut1 mRNA and/or protein expression (Yang et al., 2013; Zhou et al., 2017; Popović et al., 2019). However, only one study demonstrated increased Glut1 activation by telmisartan (Zhou et al., 2017), with the other two compounds being associated with Glut1 suppression.

The remaining 32 activators and seven inhibitors identified from the pilot library represent classes of large numbers of derivatives and are novel. To our knowledge, they have not been studied preclinically or in cell lines or animals. The effect of these compounds on glucose transport is similar to or greater than those above.

We used ventral-view videos of spontaneous mouse locomotion. Quantification of the motor difficulties of G1D patients has remained elusive. Our deep learning-based approach for quantifying various performance parameters in G1D mice may be applicable to patients. Using DeepLabCut (Mathis et al., 2018; Nath et al., 2019), we have generated a robust tool for G1D mouse part tracking. Glucose administration provided proof of concept for the automated tracking of mouse behavior and validated the expanded locomotor parameter

set. Importantly, 55% of the parameters of the set reported differences between control and G1D mice. After glucose administration, the speed parameters were significantly lower even for a small stretch of run on the track (half lap). This, along with a lower rate of change of speed, also suggests that glucose induces a more balanced and stable gait, similar to baclofen. Strikingly, one-way multivariate analysis of variance test on PCA values for all comparisons yielded a significant cluster separation for both saline and glucose injection when compared with baseline, both for control and G1D mice. Intraperitoneal injections can cause motor performance changes (Lapin, 1995), and this may account for the cluster separation for baseline and saline in both groups of mice. We found that a significant sex difference in body weight for G1D mice might account for the sex dependence of the glucose and motor effects (Supplemental Fig. 1). Another cause could be a sex difference in renal Glut1 expression level. Notably, even with a relatively small sample size ($n = 5$ mice in each group), our methodology was robust enough to discern gender differences in foot speed and rate of change of speed at baseline associated with a difference in blood glucose concentration. Nevertheless, a greater number of mice would likely be needed for further motor analyses based on sex.

Among our activator drugs, some have been sporadically used in G1D. However, in all likelihood, ineffective drugs remain unreported. In this context, acetazolamide has been used to treat episodic motor and other dysfunction (Anheim et al., 2011; Chambon et al., 2013; Ramm-Pettersen et al., 2013; Tchapyjnikov and Mikati, 2018) ($n = 71$ patient observations in G1D epilepsy; J. M. Pascual, unpublished data). This is based on an unsystematic, trial-and-error approach (Klepper et al., 2020; Cervenka et al., 2021). Caution must be exercised to assign beneficial or detrimental effects to isolated locomotor features. For example, 1 hour after acetazolamide administration, several mouse performance parameters exhibited a 'negative' or deviating from normal impact. We observed an increase in stationary gait-width after 1 hour of acetazolamide injection that persisted for 5 hours. Increase in gait width has been associated with lesions (Gadalla et al., 2014), but see below.

Another example of transport activator used in G1D is baclofen, which has been employed for a movement disorder (Hanci et al., 2018) ($n = 8$ patient observations; J. M. Pascual, unpublished data), but sedation has precluded further evaluation. One hour after baclofen administration, G1D mouse average swing speed decreases and is close to attaining significance. Stride length decreases significantly. This may indicate that the mice increase balance by reducing the vertical center of mass motion as humans do (Orendurff et al., 2004), signifying a more balanced gait, with the mice taking slower or more steady steps relative to the rapid and excessively fragmented gait characteristic of G1D mice.

These observations help situate the locomotor parameter evaluation into context. Human gait is a dynamic composite of multiple postural relations such that a change in a parameter does not necessarily convey a negative impact on locomotion. For example, broadening of gait may be considered a compensation for, rather than a manifestation of, the mechanism responsible for ataxia. Attempting locomotion with a narrow gait base in ataxia can lead to falls. Thus, further studies may be necessary to elucidate the overall impact of a drug on human locomotion when this cannot be directly inferred from mouse data.

In conclusion, we have identified compounds with significant potential to stimulate or inhibit cellular glucose transport and have developed a method to assess their whole-organism impact via automated mouse behavioral analysis. To our knowledge, few or no stimulators have been previously described. However, the screening approach we used for the activators does not differentiate between increased kinetics of glucose transport at the individual transporter level versus increased levels of overall protein, among other molecular mechanism possibilities. The same considerations apply to inhibitors. Thus, future work will study the compounds at a mechanistic level. Mechanism is important in G1D because disease-causing mutations may act via a variety of effects, including changes in Glut1 production, posttranslational modification, localization, regulation, aggregation, recycling from the cell membrane, or catalytic activity (Pascual et al., 2008; Lee et al., 2015; Meyer et al., 2018); and these may prove differentially susceptible to drug modulation. This diversity in mechanistic selectivity may not be as relevant in non-genetic forms of Glut1 dysfunction such as dementia, where the nature of Glut1 dysfunction is more uniform and activation via one, or more than one but homogeneous pharmacological mechanisms may be sufficient for clinical benefit. It is possible that the identified compounds target multiple mechanisms. In this instance, leveraging different Glut1 or glucose transport activation or suppression mechanisms may enable synergistic combination therapies. Overall, the drugs for which clinical or preclinical data exist have the greatest potential to prove useful in brain glucose deficiency disorders. However, the drugs from the pilot library and their derivative compounds may represent a greater long-term opportunity to identify a larger array of high-potency Glut1 or glucose transport activators and inhibitors.

Authorship Contributions

Participated in research design: Posner, Park, Pascual.
Conducted experiments: Kathote, Ma, Angulo, Chen.
Contributed new reagents or analytic tools: Kathote, Chen, Jakkamsetti, Dobariya, Good, Posner.
Performed data analysis: Kathote, Ma, Chen, Jakkamsetti.
Wrote or contributed to the writing of the manuscript: Kathote, Angulo, Posner, Park, Pascual.

References

Akman CI, Engelstad K, Hinton VJ, Ullner P, Koenigsberger D, Leary L, Wang D, and De Vivo DC (2010) Acute hyperglycemia produces transient improvement in glucose transporter type 1 deficiency. *Ann Neurol* 67:31–40.
Allaman I, Bélanger M, and Magistretti PJ (2015) Methylglyoxal, the dark side of glycolysis. *Front Neurosci* 9:23.
Anderson RE, Howard RA, and Woodbury DM (1986) Correlation between effects of acute acetazolamide administration to mice on electroshock seizure threshold and maximal electroshock seizure pattern, and on carbonic anhydrase activity in subcellular fractions of brain. *Epilepsia* 27:504–509.

Anheim M, Maillart E, Vuillaumier-Barrot S, Flamand-Rouvière C, Pineau F, Ewenczyk C, Riant F, Apartis E, and Roze E (2011) Excellent response to acetazolamide in a case of paroxysmal dyskinesias due to GLUT1-deficiency. *J Neurol* **258**:316–317.

Cervenka M, Pascual JM, Rho JM, Thiele E, Yellen G, Whittemore V, and Hartman AL (2021) Metabolism-based therapies for epilepsy: new directions for future cures. *Ann Clin Transl Neurol* **8**:1730–1737.

Chambon R, Vuillaumier-Barrot S, Seta N, Wagner S, and Sarret C (2013) Partial effectiveness of acetazolamide in a mild form of GLUT1 deficiency: a pediatric observation. *Mov Disord* **28**:1749–1751.

Cryan JF, Kelly PH, Chaperon F, Gentsch C, Mombereau C, Lingenhoehl K, Froestl W, Bettler B, Kaupmann K, and Spooren WP (2004) Behavioral characterization of the novel GABAB receptor-positive modulator GS39783 (N,N′-dicyclopentyl-2-methylsulfanyl-5-nitro-pyrimidine-4,6-diamine): anxiolytic-like activity without side effects associated with baclofen or benzodiazepines. *J Pharmacol Exp Ther* **310**:952–963.

Czuczwar SJ, Ikonomidou C, Kleinrok Z, Turski L, and Turski W (1986) Effect of aminophylline on the protective action of common antiepileptic drugs against electroconvulsions in mice. *Epilepsia* **27**:204–208.

DeBerardinis RJ and Chandel NS (2016) Fundamentals of cancer metabolism. *Sci Adv* **2**:e1600200.

D'Souza LJ, Wright SH, and Bhattacharya D (2022) Genetic evidence that uptake of the fluorescent analog 2NBDG occurs independently of known glucose transporters. *PLoS One* **17**:e0261801.

Ebenezer IS and Prabhaker M (2007) The effects of intraperitoneal administration of the GABA(B) receptor agonist baclofen on food intake in CFLP and C57BL/6 mice. *Eur J Pharmacol* **569**:90–93.

Gadalla KK, Ross PD, Riddell JS, Bailey ME, and Cobb SR (2014) Gait analysis in a Mecp2 knockout mouse model of Rett syndrome reveals early-onset and progressive motor deficits. *PLoS One* **9**:e112889.

Goodwin J, Neugent ML, and Kim JW (2017a) Lung squamous cell carcinoma exhibits a targetable glucose dependency unique among non-small cell lung cancers. *Mol Cell Oncol* **4**:e1364211.

Goodwin J, Neugent ML, Lee SY, Choe JH, Choi H, Jenkins DMR, Ruthenborg RJ, Robinson MW, Jeong JY, Wake M, et al. (2017b) The distinct metabolic phenotype of lung squamous cell carcinoma defines selective vulnerability to glycolytic inhibition. *Nat Commun* **8**:15503.

Hamilton KE, Bouwer MF, Louters LL, and Looyenga BD (2021) Cellular binding and uptake of fluorescent glucose analogs 2-NBDG and 6-NBDG occurs independent of membrane glucose transporters. *Biochimie* **190**:1–11.

Hanci I, Kamm C, Scholten M, Roncoroni LP, Weber Y, Krüger R, Plewnia C, Gharabaghi A, and Weiss D (2018) Long-term effect of GPi-DBS in a patient with generalized dystonia due to GLUT1 deficiency syndrome. *Front Neurol* **9**:381.

Hao J, Kelly DI, Su J, and Pascual JM (2017) Clinical aspects of glucose transporter type 1 deficiency: information from a global registry. *JAMA Neurol* **74**:727–732.

Heilig CW, Saunders T, Brosius 3rd FC, Moley K, Heilig K, Baggs R, Guo L, and Conner D (2003) Glucose transporter-1-deficient mice exhibit impaired development and deformities that are similar to diabetic embryopathy. *Proc Natl Acad Sci USA* **100**:15613–15618.

Ichikawa N, Naora K, Hirano H, and Iwamoto K (1998) Quantitation of acetazolamide in rat plasma, brain tissue and cerebrospinal fluid by high-performance liquid chromatography. *J Pharm Biomed Anal* **17**:1415–1421.

Jakkamsetti V, Scudder W, Kathote G, Ma Q, Angulo G, Dobariya A, Rosenberg RN, Beutler B, and Pascual JM (2021) Quantification of early learning and movement sub-structure predictive of motor performance. *Sci Rep* **11**:14405.

Jones TR, Kang IH, Wheeler DB, Lindquist RA, Papallo A, Sabatini DM, Golland P, and Carpenter AE (2008) CellProfiler Analyst: data exploration and analysis software for complex image-based screens. *BMC Bioinformatics* **9**:482.

Klepper J, Akman C, Armeno M, Auvin S, Cervenka M, Cross HJ, De Giorgis V, Della Marina A, Engelstad K, Heussinger N, et al. (2020) Glut1 deficiency syndrome (Glut1DS): state of the art in 2020 and recommendations of the international Glut1DS study group. *Epilepsia Open* **5**:354–365.

Koy A, Assmann B, Klepper J, and Mayatepek E (2011) Glucose transporter type 1 deficiency syndrome with carbohydrate-responsive symptoms but without epilepsy. *Dev Med Child Neurol* **53**:1154–1156.

Lapin IP (1995) Only controls: effect of handling, sham injection, and intraperitoneal injection of saline on behavior of mice in an elevated plus-maze. *J Pharmacol Toxicol Methods* **34**:73–77.

Lee EE, Ma J, Sacharidou A, Mi W, Salato VK, Nguyen N, Jiang Y, Pascual JM, North PE, Shaul PW, et al. (2015) A protein kinase C phosphorylation motif in GLUT1 affects glucose transport and is mutated in GLUT1 deficiency syndrome. *Mol Cell* **58**:845–853.

Li X, Risbrough VB, Cates-Gatto C, Kaczanowska K, Finn MG, Roberts AJ, and Markou A (2013) Comparison of the effects of the GABAB receptor positive modulator BHF177 and the GABAB receptor agonist baclofen on anxiety-like behavior, learning, and memory in mice. *Neuropharmacology* **70**:156–167.

Lipinski CA, Lombardo F, Dominy BW, and Feeney PJ (2001) Experimental and computational approaches to estimate solubility and permeability in drug discovery and development settings. *Adv Drug Deliv Rev* **46**:3–26.

Marin-Valencia I, Good LB, Ma Q, Duarte J, Bottiglieri T, Sinton CM, Heilig CW, and Pascual JM (2012) Glut1 deficiency (G1D): epilepsy and metabolic dysfunction in a mouse model of the most common human phenotype. *Neurobiol Dis* **48**:92–101.

Marin-Valencia I, Good LB, Ma Q, Malloy CR, and Pascual JM (2013) Heptanoate as a neural fuel: energetic and neurotransmitter precursors in normal and glucose transporter I-deficient (G1D) brain. *J Cereb Blood Flow Metab* **33**:175–182.

Mathis A, Mamidanna P, Cury KM, Abe T, Murthy VN, Mathis MW, and Bethge M (2018) DeepLabCut: markerless pose estimation of user-defined body parts with deep learning. *Nat Neurosci* **21**:1281–1289.

Mathis A, Schneider S, Lauer J, and Mathis MW (2020) A primer on motion capture with deep learning: principles, pitfalls, and perspectives. *Neuron* **108**:44–65.

Meyer K, Kirchner M, Uyar B, Cheng JY, Russo G, Hernandez-Miranda LR, Szymborska A, Zauber H, Rudolph IM, Willnow TE, et al. (2018) Mutations in disordered regions can cause disease by creating dileucine motifs. *Cell* **175**:239–253.e17.

Nath T, Mathis A, Chen AC, Patel A, Bethge M, and Mathis MW (2019) Using DeepLabCut for 3D markerless pose estimation across species and behaviors. *Nat Protoc* **14**:2152–2176.

Orendurff MS, Segal AD, Klute GK, Berge JS, Rohr ES, and Kadel NJ (2004) The effect of walking speed on center of mass displacement. *J Rehabil Res Dev* **41**:829–834.

Parolin G, Drigo P, Toldo I, Boniver C, Gatta M, Burlina A, Laverda AM, and Sartori S (2011) Pre- and postprandial electroencephalography in glucose transporter type 1 deficiency syndrome: an illustrative case to discuss the concept of carbohydrate responsiveness. *J Child Neurol* **26**:103–108.

Pascual JM, Liu P, Mao D, Kelly DI, Hernandez A, Sheng M, Good LB, Ma Q, Marin-Valencia I, Zhang X, et al. (2014) Triheptanoin for glucose transporter type I deficiency (G1D): modulation of human ictogenesis, cerebral metabolic rate, and cognitive indices by a food supplement. *JAMA Neurol* **71**:1255–1265.

Pascual JM and Ronen GM (2015) Glucose transporter type I deficiency (G1D) at 25 (1990-2015): presumptions, facts, and the lives of persons with this rare disease. *Pediatr Neurol* **53**:379–393.

Pascual JM, Van Heertum RL, Wang D, Engelstad K, and De Vivo DC (2002) Imaging the metabolic footprint of Glut1 deficiency on the brain. *Ann Neurol* **52**:458–464.

Pascual JM, Wang D, Yang R, Shi L, Yang H, and De Vivo DC (2008) Structural signatures and membrane helix 4 in GLUT1: inferences from human blood-brain glucose transport mutants. *J Biol Chem* **283**:16732–16742.

Perles-Barbacaru TA, Procissi D, Demyanenko AV, and Jacobs RE (2012) Quantitative pharmacologic MRI in mice. *NMR Biomed* **25**:498–505.

Popović KJ, Popović DJ, Miljković D, Lalošević D, Čapo I, and Popović JK (2019) Physicochemical and pathohistological changes in experimental fibrosarcoma tumors of hamsters treated with metformin and itraconazole. *Oncol Lett* **18**:1697–1712.

Rajasekaran K, Ma Q, Good LB, Kathote G, Jakkamsetti V, Liu P, Avila A, Primeaux S, Enciso Alva J, Markussen KH, et al. (2022) Metabolic modulation of synaptic failure and thalamocortical hypersynchronization with preserved consciousness in Glut1 deficiency. *Sci Transl Med* **14**:eabn2956.

Ramm-Pettersen A, Nakken KO, Skogseid IM, Randby H, Skei EB, Bindoff LA, and Selmer KK (2013) Good outcome in patients with early dietary treatment of GLUT-1 deficiency syndrome: results from a retrospective Norwegian study. *Dev Med Child Neurol* **55**:440–447.

Rosenberg RN and Pascual JM (2020) *Rosenberg's Molecular and Genetic Basis of Neurological and Psychiatric Disease*, 6th ed, vol. 1, Academic Press, Cambridge, MA.

Shishov N, Elabd K, Komisar V, Chong H, and Robinovitch SN (2021) Accuracy of Kinovea software in estimating body segment movements during falls captured on standard video: effects of fall direction, camera perspective and video calibration technique. *PLoS One* **16**:e0258923.

Sinclair LV, Barthelemy C, and Cantrell DA (2020) Single cell glucose uptake assays: a cautionary tale. *Immunometabolism* **2**:e200029.

Szczygielski J, Hubertus V, Kruchten E, Müller A, Albrecht LF, Mautes AE, Schwerdtfeger K, and Oertel J (2019) Brain edema formation and functional outcome after surgical decompression in murine closed head injury are modulated by acetazolamide administration. *Front Neurol* **10**:273.

Tchapyjnikov D and Mikati MA (2018) Acetazolamide-responsive episodic ataxia without baseline deficits or seizures secondary to GLUT1 deficiency: a case report and review of the literature. *Neurologist* **23**:17–18.

Varani AP, Moutinho Machado L, and Balerio GN (2014) Baclofen prevented the changes in c-Fos and brain-derived neutrophic factor expressions during mecamylamine-precipitated nicotine withdrawal in mice. *Synapse* **68**:508–517.

von Moers A, Brockmann K, Wang D, Korenke CG, Huppke P, De Vivo DC, and Hanefeld F (2002) EEG features of glut-1 deficiency syndrome. *Epilepsia* **43**:941–945.

Wang D, Pascual JM, and De Vivo D (1993) Glucose transporter type 1 deficiency syndrome, in *GeneReviews* (Adam MP, Ardinger HH, Pagon RA, Wallace SE, Bean LJH, Stephens K, and Amemiya A, eds) vol. R, University of Washington, Seattle, WA.

Wang D, Pascual JM, Yang H, Engelstad K, Mao X, Cheng J, Yoo J, Noebels JL, and De Vivo DC (2006) A mouse model for Glut-1 haploinsufficiency. *Hum Mol Genet* **15**:1169–1179.

Wu Z, Liu D, and Sui Y (2008) Quantitative assessment of hit detection and confirmation in single and duplicate high-throughput screenings. *J Biomol Screen* **13**:159–167.

Yang Y, Wolfram J, Boom K, Fang X, Shen H, and Ferrari M (2013) Hesperetin impairs glucose uptake and inhibits proliferation of breast cancer cells. *Cell Biochem Funct* **31**:374–379.

Zhang JH, Chung TDY, and Oldenburg KR (1999) A simple statistical parameter for use in evaluation and validation of high throughput screening assays. *J Biomol Screen* **4**:67–73.

Zhang Y, Zhang S, Marin-Valencia I, and Puchowicz MA (2015) Decreased carbon shunting from glucose toward oxidative metabolism in diet-induced ketotic rat brain. *J Neurochem* **132**:301–312.

Zhao Z, Wang L, Gao W, Hu F, Zhang J, Ren Y, Lin R, Feng Q, Cheng M, Ju D, et al. (2017) A central catecholaminergic circuit controls blood glucose levels during stress. *Neuron* **95**:138–152.e5.

Zhou J, Burns MP, Huynh L, Villapol S, Taub DD, Saavedra JM, and Blackman MR (2017) Temporal changes in cortical and hippocampal expression of genes important for brain glucose metabolism following controlled cortical impact injury in mice. *Front Endocrinol (Lausanne)* **8**:231.

Address correspondence to: Dr. Juan M. Pascual, Director, Rare Brain Disorders Program, University of Texas Southwestern Medical Center, 5323 Harry Hines Boulevard Stop 8813, Dallas, TX 75390-8813. E-mail: Juan.Pascual@utsouthwestern.edu; or Jason Y. Park, University of Texas Southwestern Medical Center, 5323 Harry Hines Boulevard, Dallas, TX 75390. E-mail: Jason.Park@UTSouthwestern.edu